Pergamon

PII: S0191-8141(96)00037-5

*Journal of Structural Geology*, Vol. 18, No. 9, pp. 1151 to 1166, 1996

0191-8141/96 $15.00+0.00

# Differential stress control on the growth and orientation of flame perthite: a palaeostress-direction indicator

L. L. PRYER* and P.-Y. F. ROBIN

Department of Geology, Erindale College, University of Toronto, Mississauga, Ontario, Canada, L5L 1C6

(*Received* 9 *June* 1995; *accepted in revised form* 11 *April* 1996)

**Abstract**—Albite flames result from the replacement of K-feldspar by albite through alkali exchange. In flame perthites from deformed granites within the Grenville Front Tectonic Zone, replacement is driven by retrograde breakdown of plagioclase and hydration of K-feldspar. Within the strain fabric of the host rock, albite flames preferentially form subparallel to the inferred maximum compression direction and also develop at high-stress points such as grain-to-grain contacts. Flame tips are generally parallel to the 'normal' perthite crystallographic direction, i.e. the Murchison plane, which is the orientation of the plane of minimum crystallographic lattice misfit between the albite and K-feldspar.

We propose that the morphology of an albite flame is controlled by the coherent propagation of its tip into the K-feldspar crystal lattice, and that the orientation of the flames with respect to the rock fabric is controlled by the differential stress imposed during metamorphism. This type of replacement requires dry conditions in which there would be inefficient dissolution–reprecipitation along completely incoherent interfaces (normal replacement), and increased strength of feldspar. Under these conditions coherency is maintained to avoid a very large kinetic barrier.

The differences in lattice misfit along the Murchison plane between K-feldspar and albite requires either high elastic strain energy (if the fit is coherent), or lattice dislocation energy (if the fit is semi-coherent). Such energy might be expected to inhibit the replacement growth of albite lamellae in a host feldspar. However, compression parallel to the Murchison plane reduces the lattice misfit along the compression direction. This results (1) in an increase in the Helmholtz free energy of the K-feldspar, and (2) in a reduction in the Helmholtz energy of the albite lamellae or of the semi-coherent interface. Thus, albite replacement allows a decrease in net free energy without the destruction of the alumino–silicate framework and is therefore favoured under conditions of high differential stress. Since flame growth is controlled by the imposed differential stress and not by strain in the host rock, flame perthite has potential as a palaeostress-direction indicator. 

## INTRODUCTION

Flame perthite (Fig. 1) is one of many morphologies of K-feldspar and albite intergrowths, but differs from most other perthite morphologies in that it is generally found in deformed quartzo–feldspathic rocks (e.g. Debat *et al.* 1978, Passchier 1982, Stel 1986). The origin of flame perthite has been attributed to various processes including exsolution (e.g. Passchier 1982), replacement (e.g. Smithson 1963) and open space filling (Debat *et al.* 1978). Debat *et al.* (1978) also noted that albite lamellae had apparently formed parallel to the inferred direction of maximum compressive stress during shearing of the host K-feldspar, and concluded that the flames must have developed as albite filled tension gashes. Pryer *et al.* (1995) have demonstrated this same relationship between the flame orientation and maximum stress direction, but Pryer & Robin (1995) have shown, on the basis of microprobe analyses and mineral equilibria, that flame perthite has a replacement origin. In the rocks we have examined, replacement was an exchange reaction driven by two retrograde reactions: saussuritization of calcic plagioclase, and hydration of K-feldspar.

In addition to the preferred orientation relative to the host-rock fabric, flames also have a specific crystallographic relationship with the K-feldspar host. The albite and the K-feldspar share the same crystallographic lattice orientation (Pryer *et al.* 1995), and the crystallographic plane defined by the tips of the flames coincides with that of cryptoperthite and many other perthites of exsolution origin.

In this paper, we propose a mechanism for flame growth which accounts for: (1) the morphology of the flames, (2) their orientation within the K-feldspar crystal structure and (3) their orientation with respect to the rock fabric. The model for the flame morphology and crystallographic orientation expands on a suggestion by Smith (1974, p.177), which was based on the observations of Petrović (1973), in which the tip of a wedge-shaped albite replacement front retains coherency as it moves through the K-feldspar lattice. The orientation of flames with respect to the rock fabric is controlled by the externally imposed compressive stress, reducing the lattice dimensions in the K-feldspar thereby reducing the coherency stress in the albite. Since flame perthites have the same crystallographic relationship as cryptoperthites, it is useful here to review the phenomenology of cryptoperthites.

### *Cryptoperthites*

Cryptoperthites (optically invisible, $<0.5\ \mu m$ lamellae) have nearly parallel K-feldspar and albite lattices and approximately constant orientation of the intergrowth interface. The interface orientation was first determined optically for moonstones by Bøggild (1924), and later confirmed by X-ray studies (Laves 1952, Smith 1961) and Transmission Electron Microscopy (TEM). The interface orientation is generally parallel to an irrational crystal-

*Present address: Research School of Earth Sciences, Australian National University, Canberra ACT 0200, Australia.

lographic plane between ($\bar{6}01$) and ($\bar{8}01$), but the orientation may vary depending on composition (Brown & Willaime 1974). The perthite plane is commonly referred to as the Murchison plane (Smith 1974, after a variety of moonstone described as murchisonite in 1828).

X-ray analysis (Smith 1961) and TEM show that in most cryptoperthites the interfaces are coherent (e.g. Aberdam 1965, Gandais *et al.* 1974, Robin 1974, Brown & Parsons 1984), meaning that the two phases maintain continuity of their lattices along the interface (Fig. 2, Yund 1983). Coherency imposes anomalous lattice parameters in both host and lamellae and it thus requires that there be large internal stresses* in order to maintain these parameters. Smith (1961) noted that this preferred interface orientation is that for which the misfit between the lattices is minimum. Therefore, the cryptoperthite orientation has a total elastic strain energy (i.e. the combined strain energy of both the albite and K-feldspar lattices) which is a minimum (Willaime *et al.* 1973, Robin 1974).

The elastic strain energy due to coherency is significant, even in the minimum energy orientation. In particular, for a very small proportion of pure albite lamellae within a microcline ($Or_{95}$), the tensile stress within the albite will be 2.0 GPa parallel to the *b*-axis and 0.9 GPa along a direction orthogonal to *b*, within the lamella. If the lamella are in orthoclase the stresses are 2.3 and 0.6 GPa, respectively (Appendix B). The corresponding elastic strain energy is *ca.* 2 kJ mole$^{-1}$ of albite. Coherent cryptoperthite lamellae are thus metastable. They only form during relatively rapid exsolution because of the resistance to long-range diffusion of Na and K, or to the formation of an incoherent boundary within the crystal does not permit incoherent growth. Whenever kinetically possible, lamellae lose coherency to yield unstrained phases.

*Loss of coherency*

Prior to the experimental observations of coherency, Bollmann & Nissen (1968) had noted that the orientation of cryptoperthite lamellae could be explained as the orientation which minimised the energy of misfit lattice dislocations located along the interfaces between semi-coherent lamellae. This is because both the coherency and the semi-coherency models determine the direction of the minimum difference in repeat distances along the interface. For a coherent interface, the surface energy is negligible compared to the elastic strain energy, and therefore the additional energy of a coherent lamella is proportional to its volume. On the other hand, the additional energy of a semi-coherent lamella is proportional to its surface area. This contrast forms the basis of the qualitative explanations for the loss of coherency of exsolution lamellae as they become wide (Yund 1983). But, as discussed by Brown & Parsons (1984), the dislocations in lamellar interfaces of microperthites are rare, and are apparently controlled by the overall composition of the alkali feldspar. Thus, the presence of dislocations cannot necessarily be assumed. Dislocations have been found in lamellae of K-feldspar with bulk compositions greater than 60–70% Or (Gandais *et al.* 1974, Brown & Parsons 1983) and in ternary mesoperthite with high An contents (Brown & Parsons 1984).

*Coherent replacement in flame perthite*

Pryer *et al.* (1995) show that the crystallographic relationship between the albite flames and the surrounding K-feldspar is similar to some cryptoperthites: (1) the crystallographic orientation of the albite is the same as that of the K-feldspar; and (2) the orientation of the interface near the flame tips is the Murchison plane. Thus, the development of the flame perthite must be controlled by lattice misfit. But flame perthites form by *replacement*, not by exsolution (Pryer & Robin 1995). Coherent replacement would appear to be unlikely: why would the albite component choose to form a coherent (or semi-coherent) lamella in a K-feldspar at the thermodynamic cost of 2 kJ mol$^{-1}$ rather than forming unstrained albite at the periphery of the K-feldspar?

The orientation of the lamellae with respect to the rock fabric indicates that they formed approximately parallel to the inferred direction of the maximum principal compressive stress responsible for that fabric (Pryer *et al.* 1995). This observation suggests that the stress somehow assists flame growth and control flame orientation. In the model presented here we propose that, within a crystal subjected to a differential stress, replacement can proceed along a coherent interface.

Coherent replacement achieves minimal disruption of the bonds within the lattice by maintaining the Al–Si framework essentially intact. The 'kinetic argument' is thus the same as that for coherent exsolution: by avoiding the creation of a new incoherent (and therefore high energy) surface, replacement can occur faster and with a lower energy budget. However, as explained below, an appropriate external stress on the host crystal promotes coherent propagation of a flame tip.

## FIELD RELATIONS AND PETROGRAPHY

The Grenville Front Tectonic Zone (GFTZ) is a crustal-scale reverse offset shear zone in which rocks of the Grenville Province have been thrust over rocks of the Southern, Superior, Nain and Churchill Provinces of the Canadian Shield (Wynne-Edwards 1972). The samples used in this study are from a section of the GFTZ, 20–30 km NE of Killarney in SW Ontario, Canada. Timing of metamorphism and cooling in the Killarney area has been determined by Haggart *et al.* (1993).

In the sampled area, granitic protoliths have been deformed to varying bulk strains under metamorphic

*Note that the convention used in this paper is that stresses and strains within the crystals are negative for compression and positive for extension. This is done so that a decrease in lattice spacing equates to a negative strain. Externally imposed tectonic stresses are expressed in the usual convention with compressive stress being positive. In Appendix B, the sign of the external stress is reversed in the calculations.

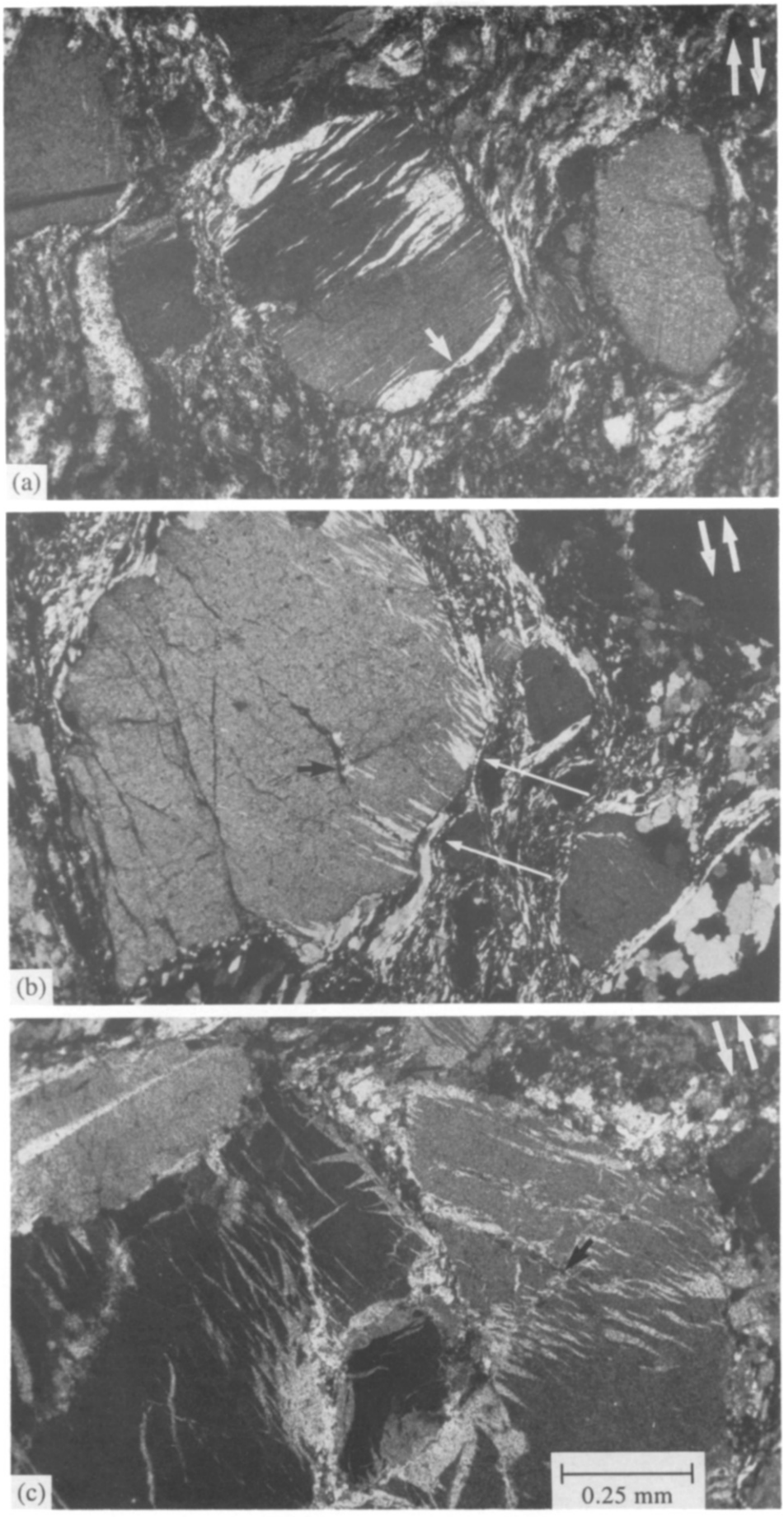


Fig. 1. Photomicrographs of flame perthite. Flame long axes trend subnormal to the foliation direction shown as shear sense arrows in the top right of each photo. (a) Well-rounded K-feldspar grain with a change in orientation in the middle of the grain, evident by the change in extinction. Albite flames are well developed only in the top half of the grain. Albite also occurs at grain ends in normal pressure-shadow locations (arrow). (b) Preferential flame development at high stress points along the grain boundary (long arrows) where feldspar grains in the matrix are in close contact to the host K-feldspar. Some flame development also occurs at a fracture within the grain (black arrow). (c) Albite replacement along all grain boundaries in contacts with another feldspar grain. Flames also occur along fractures (black arrow). Flames may develop in orientations other than the Murchison plane. Scale bar 0.25 mm, same for (a), (b) and (c).

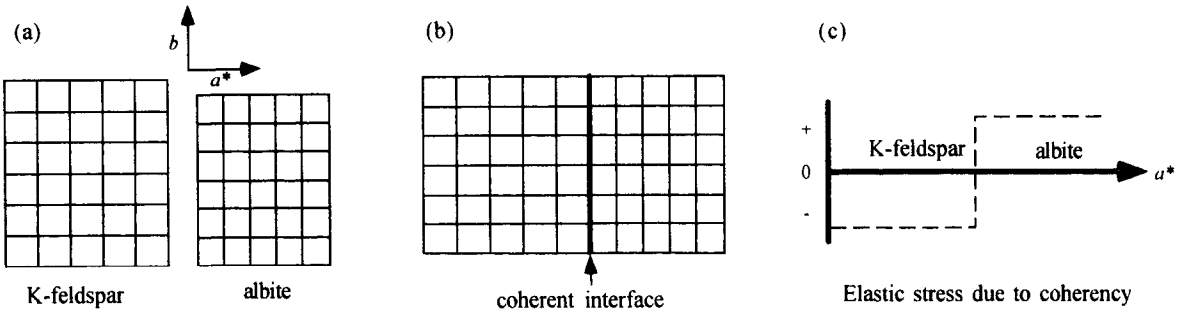


Fig. 2. (a) Schematic representation of the lattices of unstressed K-feldspar and albite. (b) Stressed lattices joined at a coherent interface parallel to (010). (c) The elastic stress (*ca.* 1–2 GPa) required to maintain coherency shown in (b) is shared between the two phases. In the sign convention used, tension is positive and compression negative.

grade ranging from sub-greenschist to upper amphibolite. Lithologies vary from moderately deformed quartzo–feldspathic gneisses to ultramylonites. This area has been described elsewhere (Pryer 1985, O'Donnell 1986), and the feldspar microstructures and metamorphic grade are discussed by Pryer (1993). An S–C fabric is well developed in the mylonitic rocks that form anastomosing, steeply dipping shear zones with the Grenvillian NE-trend. Between the shear zones, the extent of development of a penetrative foliation increases from NW to SE as metamorphic grade increases. Pryer (1993) has shown, on the basis of the presence of retrograde reaction products within the minerals that define the S–C fabric, that the mylonitisation of these rocks was synchronous with their retrograde metamorphism. The distribution of flame perthite in this area is generally restricted to granitic rocks deformed at greenschist grade (Pryer 1993), and correlates with brittle deformation of feldspars. The width of this zone is approximately 2 km.

In mylonites deformed at amphibolite grade within the GFTZ, flame perthite is rarely observed. However, myrmekite is ubiquitous on K-feldspar grain boundaries oriented parallel to the S-foliation, which is consistent with the observations of Vernon *et al.* (1983) and Simpson (1985). At medium-to-high metamorphic grade, myrmekite occupies the same position as flames of low-to-medium grade, and rarely, occur together.

Extensive electron microprobe analyses show K-feldspar compositions to be uniform within each sample regardless of flame content at the 1$\mu$m scale. Across the field area K-feldspar compositions vary from $Or_{90.3}$ at the highest grade occurrence of flames (oligoclase isograd) to $Or_{96.8}$ at the lowest (Pryer & Robin 1995, Table 1). The composition of albite flames varies only from $Ab_{97}$ to $Ab_{98}$ (Table 2). In contrast, relict plagioclase grains are highly variable, commonly ranging from albite to andesine.

Table 1. Elastic strain ($\varepsilon_i$) and stress ($\sigma_j$; GPa) values for coherent perthite lamellae.

| | Low albite–microcline | Low albite–orthoclase | High albite–sanidine* |
|---|---|---|---|
| $\varepsilon_1$ | 0.0158 | 0.0150 | 0.0182 |
| $\varepsilon_2$ | −0.0140 | −0.0168 | −0.0162 |
| $\varepsilon_3$ | −0.091 | −0.0057 | −0.0105 |
| $\varepsilon_5$ | −0.0021 | −0.0028 | −0.0024 |
| $\sigma_2$ | −1.990 | −2.338 | −2.300 |
| $\sigma_3$ | −0.920 | −0.648 | −1.060 |

*From Robin (1974).

Saussuritisation and sericitisation in plagioclase grains is ubiquitous. Those samples with the most extensive flame development also contain the most extensive alteration of plagioclase. Sericitisation in K-feldspar is rarely observed, indicating that the K-feldspar is not undergoing a hydration reaction *in situ*. Pryer & Robin (1995) conclude that albite flame growth in the K-feldspar in these rocks is the result of an exchange reaction within the K-feldspar: Na is released by the breakdown of plagioclase, and K consumed by the growing muscovite (as sericite) within the plagioclase (Fig. 3). Growth of sericite within the plagioclase implies mobility of K and Na relative to Al.

Using an initial plagioclase composition of $An_{20}$, the overall reaction can be summarised as:

$$20 \text{ oligoclase} + 1\text{K-feldspar} + 2H_2O$$
$$= 2 \text{ zoisite} + \text{muscovite} + 2\text{quartz}$$
$$+15 \text{ albite}_{\text{plagioclase}} + 1\text{albite}_{\text{flame}} \quad (1)$$

but, within the alkali feldspar, the reaction is:

$$\text{plagioclase} + 0.5Na_2O + 1\text{K-feldspar}$$
$$= 1\text{albite}_{\text{flame}} + 0.5K_2O\text{-sericite}. \quad (2)$$

This model does not require any Al–Si exchange. $Na_2O$, $K_2O$, and $H_2O$ are the only components that must migrate between grains, allowing $Al_2O_3$ and $SiO_2$ to remain within the altering plagioclase grain.

The temperature and extent of replacement depends on when, and how much, water infiltrates the rock. The aqueous fluid pressure may have been significantly lower than lithostatic pressure during flame growth (see discussion in Pryer & Robin 1995).

## FLAME DISTRIBUTION AND ORIENTATION

Albite flames most commonly extend inward from K-feldspar grain boundaries (Figs. 1a & b), internal

Table 2. Elastic strain energy in kJ mol$^{-1}$; for compressive stress ($\sigma^b_{1,i}$) in GPa

| | $f^{ab}$ | $\sigma^b = 0$ | $\sigma_{1,2}{}^b = 0.5$ | $\sigma_{1,2}{}^b = 1.0$ | $\sigma_{1,3}{}^b = 0.5$ | $\sigma_{1,3}{}^b = 1.0$ | $\sigma_{1,3}{}^b = 1.0$ $P_c = 250$ | $\sigma_{1,1}{}^b = 0.5$ | $\sigma_{1,1}{}^b = 1.0$ |
|---|---|---|---|---|---|---|---|---|---|
| Microcline | 0 | 0 | 0.09 | 0.37 | 0.14 | 0.58 | 0.49 | 0.37 | 1.47 |
| | 0.2 | 0.07 | 0.31 | 0.73 | 0.32 | 0.84 | 0.74 | 0.36 | 1.39 |
| | 0.4 | 0.29 | 0.67 | 1.23 | 0.63 | 1.26 | 1.14 | 0.50 | 1.45 |
| | 0.6 | 0.65 | 1.18 | 1.88 | 1.09 | 1.82 | 1.69 | 0.78 | 1.65 |
| | 0.8 | 1.16 | 1.83 | 2.68 | 1.70 | 2.52 | 2.37 | 1.21 | 2.00 |
| | 1 | 1.81 | 2.62 | 3.62 | 2.45 | 3.37 | 3.21 | 1.79 | 2.50 |
| Albite | 0 | 1.81 | 1.19 | 0.75 | 1.46 | 1.40 | 1.40 | 2.57 | 4.07 |
| | 0.2 | 1.16 | 0.68 | 0.38 | 0.91 | 0.95 | 0.92 | 1.84 | 3.26 |
| | 0.4 | 0.65 | 0.31 | 0.16 | 0.50 | 0.64 | 0.60 | 1.26 | 2.60 |
| | 0.6 | 0.29 | 0.10 | 0.08 | 0.24 | 0.47 | 0.42 | 0.82 | 2.08 |
| | 0.8 | 0.07 | 0.02 | 0.16 | 0.12 | 0.45 | 0.38 | 0.52 | 1.70 |
| | 1.0 | 0 | 0.09 | 0.37 | 0.14 | 0.57 | 0.49 | 0.37 | 1.47 |
| Total ($F_T{}^{el,b}$) (symmetic across $f^{ab} = 0.5$) | 0 | 0 | 0.09 | 0.37 | 0.14 | 0.58 | 0.49 | 0.37 | 1.47 |
| | 0.1 | 0.16 | 0.26 | 0.53 | 0.31 | 0.74 | 0.65 | 0.53 | 1.64 |
| | 0.2 | 0.29 | 0.38 | 0.66 | 0.43 | 0.86 | 0.78 | 0.66 | 1.76 |
| | 0.3 | 0.38 | 0.47 | 0.75 | 0.52 | 0.96 | 0.87 | 0.75 | 1.85 |
| | 0.4 | 0.43 | 0.53 | 0.80 | 0.58 | 1.01 | 0.92 | 0.80 | 1.91 |
| | 0.5 | 0.45 | 0.54 | 0.82 | 0.60 | 1.03 | 0.94 | 0.82 | 1.93 |

All results calculated for atmospheric pressure, $P_c$ = 0.1 MPa (except column 7 where $P_c$ = 250 MPa), plus a directed external compressive stress $\sigma^b_{1,i}$.

fractures and microfaults (Fig. 1c). Flames taper within each grain and are generally widest at the grain boundaries or fractures from which they appear to emanate (Fig. 1). The density and size of flames varies within a grain as well as within a thin section. Flames may occur singly or in sets of parallel flames, and, rarely, more than one set may occur within a single grain (Fig. 1c). Albite replacement also occurs in K-feldspar grains adjacent to sites where 'pressure shadows' normally form (Fig. 1a) and at contact points between feldspar grains (Figs. 1b & c).

The majority of K-feldspar grains in the samples examined are untwinned and assumed to be orthoclase since very Or-rich K-feldspars with no obvious twinning, such as the ones observed in this study, tend to be orthoclase rather than microcline (Brown & Parsons 1984). But some perthite grains do display microcline twinning. Because of the low frequency of grains with optically visible twins, it was not possible to determine whether flames developed more frequently in microcline or orthoclase. Flames are developed in both.

Within any sample of quartzo–feldspathic mylonite not all K-feldspar grains contain flames. Some grains may exhibit more than 50% replacement by albite while others show none. For simplicity, we refer to all grains as perthitic even though, *sensu stricto*, some would be antiperthitic. The variability in amount of replacement from one K-feldspar grain to the next, within a sample, and the preferred orientation of the flames relative to the host–rock fabric indicates both crystallographic and grain orientation control over flame development.

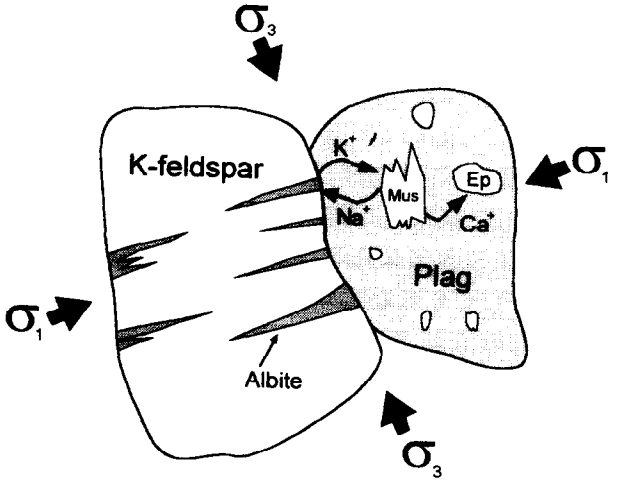


Fig. 3. Sketch showing some of the reaction products and proposed ion exchange in the hydration reaction: plag + Ksp + $H_2O$ = ep + mus + qtz + ab. Inferred external stress axes are also shown.

### *Orientation of flames within K-feldspar grains*

Pryer *et al.* (1995) have measured the preferred orientation of flames within perthitic grains using back scattered electron images and electron channelling patterns. The relationship in crystallographic orientation of the K-feldspar host and the albite flames is topotaxial. The orientation of host–flame interface for the thin, parallel-sided flame tips is essentially the same as that for cryptoperthites of exsolution origin, i.e. parallel to the *b*-axis and approximately 9° from the *c*-axis and 107° from *a*. Interfaces may vary in orientation by 20°–30° along the length of a flame where it widens away from the tip. Other orientations unrelated to the Murchison plane are found only in grains that contain multiple sets of flames. The relationship between the host and lamellae remains topotaxial for all flames regardless of the interface orientation.

*Orientation of flames with respect to the host rock fabric*

The approximate distribution of the tectonic stress at the time of deformation can be inferred from the strain fabric in the mylonites. The well-developed lineation indicates the principal extension direction (X-axis of strain) and the normal to the planar fabric gives the principal shortening direction (Z-axis of strain). The asymmetry of the S–C fabric (Fig. 4) gives the sense of shear, and therefore, a crude approximation of the principal stress directions relative to the foliation. (For the rocks described here the orientation of the external stress can be inferred from the asymmetry in the rock fabric such that the direction of maximum principal stress ($\sigma_1$) is within the quadrant sub-normal to the S-foliation, between 0 and 90° from C.)

Flame planes have a preferred orientation subnormal to the S-foliation (Fig. 4). Surfaces from which flames have grown are those subjected to high normal stress, typically subparallel to the S-foliation (Fig. 1a, see also Pryer 1993). The flames themselves trend perpendicular to these boundaries. Flames are also observed emanating from high-stress, point contacts between feldspars (Figs. 1b & c). We infer from this relationship that the flames formed with their long dimension subparallel to the external maximum compressive stress direction ($\sigma_1^b$, where $b$ denotes external bulk stress).

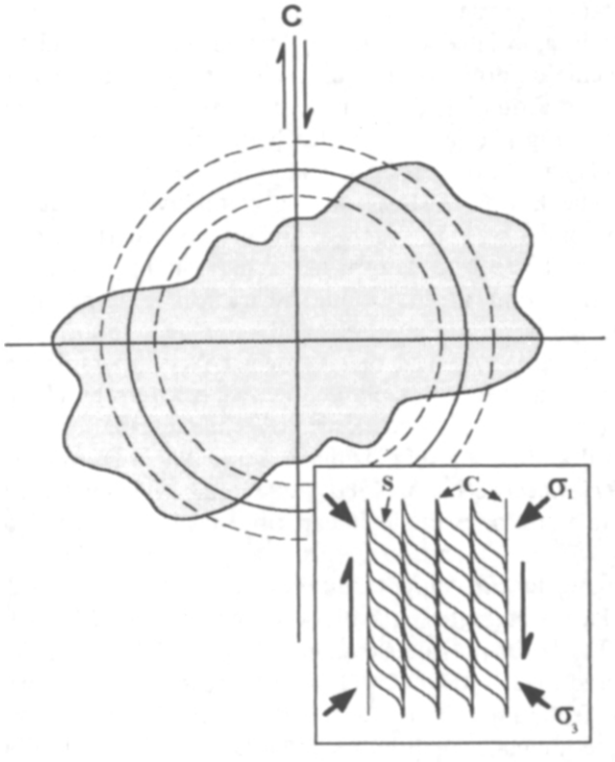


Fig. 4. Two-dimensional distribution of long axes measured in thin section of all flames ($n$ = 3222) (sample P231) relative to the foliations in the rock (inset). Flames have a strong preferred orientation subnormal to the S-foliation and subparallel to the inferred maximum compressive stress direction ($\sigma_1$). The solid circle represents the value expected for an isotropic distribution; the dashed circles correspond to departures from that value that are considered statistically significant, ie. 1.8$\sigma$ (where $\sigma$ = standard deviation).

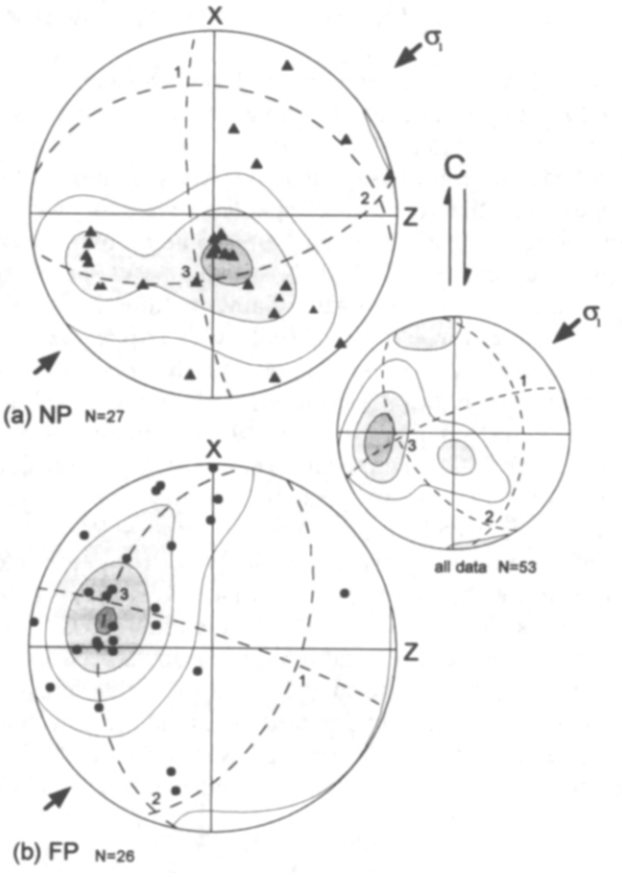


Fig. 5. Orientation of normals to the Murchison plane in 53 feldspar grains shown in equal area projection relative to the C-planes in the host rock (XY-plane of strain) with shear sense indicated. X and Z are the maximum and minimum strain axes. (a) 27 Grains with little or no perthite (NP) lamellae have the Murchison plane badly oriented for flame growth. (b) 26 Grains with well developed flame perthite lamellae (FP) have a strong preferred orientation of the Murchison plane approximately 30° from C, subparallel to the inferred $\sigma_1$ direction. Contours are 0, 2, 4 and 6$\sigma$. Also shown on each net are the 3 eigenvectors and principal planes. Data plotted using SpheriStat©.

The crystallographic orientations of 52 grains were measured by SEM electron channelling patterns (Pryer *et al.* 1995). The Murchison plane was determined for each grain and plotted as a pole in Fig. 5. Figure 5(a) shows that grains with flames have a strong crystallographic preferred orientation of their Murchison plane with respect to the inferred external stress field. Specifically, their Murchison planes are preferentially parallel to the $\sigma_1$–$\sigma_2$ plane*. Grains without flames (Fig. 5b) show no such relationship with the external stress. In other words, grains oriented with their Murchison plane parallel to the maximum stress direction have well-developed flames, whereas grains in other orientations develop only minor or no flames except at point contacts with other grains. This relationship forms the basis of the model presented below, following a discussion of the potential magnitude of the external stresses involved.

*The plunge in the maximum in Fig. 5(a) probably indicates that the section was not cut exactly parallel to the XZ-plane of strain (or the XZ-plane is not exactly parallel to $\sigma_1^b$).

## EXTERNAL STRESSES ON FELDSPAR GRAINS

The differential stress imposed on feldspars in the GFTZ at the time of deformation could have been anywhere from 0.3 to >1 GPa. These values can be justified in several ways. Differential stress on the rock (as opposed to that on the feldspar crystals) can first be estimated by grain size palaeopiezometry on quartz, (quartz abundance is 20–30% by volume of the rocks studied). For samples hosting flame perthite, the differential stresses range from 0.2 to 0.3 GPa (Appendix A).

Although such stresses appear high, they are low compared to relevant estimates of the strength of the upper crust. Ranalli & Murphy (1987) estimated a stress profile in their C(c1) model lithosphere of "... continental convergence zones, such as, for instance the Tibetan Plateau...", which is presumably applicable to the Grenville Front (e.g. Windley 1986). For the depth and temperature on that profile which corresponds to greenschist facies (25 km, 300°C), the differential stress ($\sigma_1$–$\sigma_3$), is between 0.2 and 0.5 GPa. Ranalli & Murphy (1987) assume that the top of the C(c1) model crust is relatively cool, with a hydrostatic pore fluid pressure, and its strength is therefore a pressure-dependent, but temperature- and strain-rate-independent *brittle* strength.

### *Pore fluid pressure*

The assumption of a brittle crust with a fluid pressure less than lithostatic, as in the model crust above, may seem surprising in the present situation, in which the observed metamorphic rehydration reactions (Pryer & Robin 1995) imply that there be *addition of water* into the rock. But, even though the ingress of water over large distances (from metres to kilometres) through a rock requires connected porosity (since diffusive transfer is much too slow), this does *not* require that the fluid pressure be lithostatic or even hydrostatic. In brittle deformation experiments, the pressure in dilatant pores may in fact be negligible, and there is no reason in principle that the same could not be true in nature. As explained below, the fluid pressure during partial retrograde metamorphism is not set by depth but buffered by the retrograde reactions themselves.

In the present rocks, retrograde reactions have clearly not gone to completion. Also, the rare and irregular occurrence of twinning indicates that the K-feldspar has undergone limited conversion from orthoclase to microcline; surprising if the environment were water-rich (Brown & Parsons 1993). For any 'undercooling', i.e. when the temperature is below those of the oligoclase and K-feldspar-muscovite isograds for water-saturated conditions, the activity of water is buffered to *less* than water saturation. The actual fluid pressure would depend on the activity of water, and therefore on the amount of undercooling, and on the abundance of $CO_2$. There is no petrographic evidence for $CO_2$ (e.g. carbonate) and no source of $CO_2$ is known in the vicinity. We therefore assume that fluid pressure in the open spaces is set by the activity of $H_2O$ (which is set by the amount of undercooling relative to the reaction equilibria). For reaction (1), equilibrium temperature at $H_2O$-saturation at a confining pressure, $P_c$ = 0.5 GPa, is 380°C (Pryer & Robin 1995). If water were to migrate into the rock at 340°C, i.e. an undercooling of 40°C, its activity would be buffered around 0.35. Assuming a perfect gas, this translates into a fluid pressure equal to 35% of lithostatic, which is close to the hydrostatic pressure assumed by Ranalli & Murphy (1987). It is important to note that we do not presently know the temperature at which the water was introduced into the rock. The compositions of the albite and K-feldspar can only give an approximate equilibrium temperature due to (1) the steepness of the feldspar immiscibility curves at low temperatures and (2) uncertainty in the phase boundaries. In this case, field relationships tell us that the temperature was below equilibrium for reaction (1), but not by how much. So we cannot determine the actual fluid pressure.

The above argument is of more general application than to the problem of flame perthites. It is developed here to point out that the evidence of ingress of water into the rock is not incompatible with fluid pressure less than lithostatic or hydrostatic, and therefore is not incompatible with high strength.

### *Deformation mechanisms*

The deformation mechanisms in these rocks include brittle deformation of the feldspar, the transformation strain associated with the hydration reactions, and the ductile deformation of quartz. The fine-grained matrix wraps around feldspar porphyroclasts (e.g. see Pryer 1993, Figs. 7d and 8a–c), clearly demonstrating that the feldspars are the strongest mineral in the rock.

The low flow stress of quartz relative to feldspar, combined with the high abundance of quartz, would allow the rock to deform in a ductile manner and at a higher strain rate than would a rock composed purely of feldspar (e.g. Handy 1994 and references therein). At temperatures typical of greenschist facies metamorphism, quartz deforms plastically and recovers by climb-accommodated dislocation creep while feldspar remains hard and strong (e.g. Tullis & Yund 1977, Tullis *et al.* 1979, Sacerdoti *et al.* 1980, Fitz Gerald & Stünitz 1993, Table 1). For example, in experiments at a strain rate of $\sim 10^{-5}$ $s^{-1}$, and at 400°C, a plagioclase feldspar aggregate can support differential stresses from 1.25 GPa for pressures equivalent to depths of 12–14 km to 1.9 GPa for pressures equivalent to 25–30 km (Tullis & Yund 1992). At T < 600°C, glide dislocations do not form in feldspars (Tullis & Yund 1992). Under similar experimental conditions, potassium feldspars exhibit strengths comparable to plagioclase (Willaime *et al.* 1979).

The differential stress would vary from one feldspar grain to the next, and even within a single grain, would not be constant during deformation. The local differential stress within feldspar grains would be greater than

that given by quartz palaeopiezometry or by using the estimate for crustal strength of Ranalli & Murphy (1987). Differential stresses in excess of 0.5 GPa could easily have existed at stress concentration points such as contacts between grains, and the tips of cracks or flames. The petrographic evidence of their brittle deformation suggests that the shear strength of the feldspars was reached in these rocks, and argues that locally differential stresses could have exceeded 1 GPa. The time available to natural deformation should make such a stress estimate a maximum. Crack propagation in the presence of water, and therefore brittle strength, are time-dependent (Martin 1972). Sacerdoti *et al.* (1980) point out that for natural deformation rates, dislocation glide might occur in K-feldspars at $T < 500°C$, leading to a hardened polygonal cellular structure bounded by bands with high dislocation densities. Lee *et al.* (1995) show dislocations on exsolution lamellae that form below 400°C implying that limited glide and climb is possible.

Although none of the above arguments can be used to calculate a differential stress in the feldspar grains, they are presented to demonstrate that postulating high stresses is not incompatible with the petrographic and experimental information on granitic rocks. Therefore, we assume that the differential stress within an individual feldspar grain in the GFTZ mylonites could have been between 0.3 and 1 GPa.

## THE MODEL FOR FLAME GROWTH

We propose a model as illustrated in Fig. 6. Albite flames form through the propagation of a coherent flame tip into the stressed K-feldspar lattice. Flames widen by continued replacement in the wake of the coherently propagating tip. The interface between albite and K-feldspar collects lattice dislocations as it sweeps through the crystal and becomes increasingly incoherent.

By replacing the K-feldspar, rather than nucleating albite grains as a product of the metamorphic reactions, (1) the albite is shielded by the K-feldspar from the bulk stress applied to the rock, (2) reconstruction of the Al–Si framework is not required as replacement proceeds if nucleation and growth are coherent, and (3) a volume of K-feldspar crystal with a high lattice strain energy is replaced by albite with a lower strain energy. These savings are in addition to the minimised Al and Si ionic transfers discussed in Pryer & Robin (1995).

Replacement can proceed to the extent that adjacent flames coalesce at the grain boundary or fracture and the albite is no longer shielded from the external stress by the host K-feldspar. The observation that flame development still continues, even though the albite must become stress supporting, indicates that the chemical driving force must be sufficient for the reaction to continue, once initiated. In this model we are concerned with explaining the morphology of the albite replacement; nevertheless, the driving force will be addressed further in the discussion.

As a flame widens, its boundaries are not likely to retain full coherency. There is both an increase in the number of dislocations on the interfaces and departure of lamellar orientation from the Murchison plane (Fig. 6). This configuration has been documented by Lee *et al.* (1995) in primary igneous perthites. If semi-coherency can be maintained, the flames still avoid the need to create an incoherent interface and to reconstruct the Al–Si framework as that interface migrates.

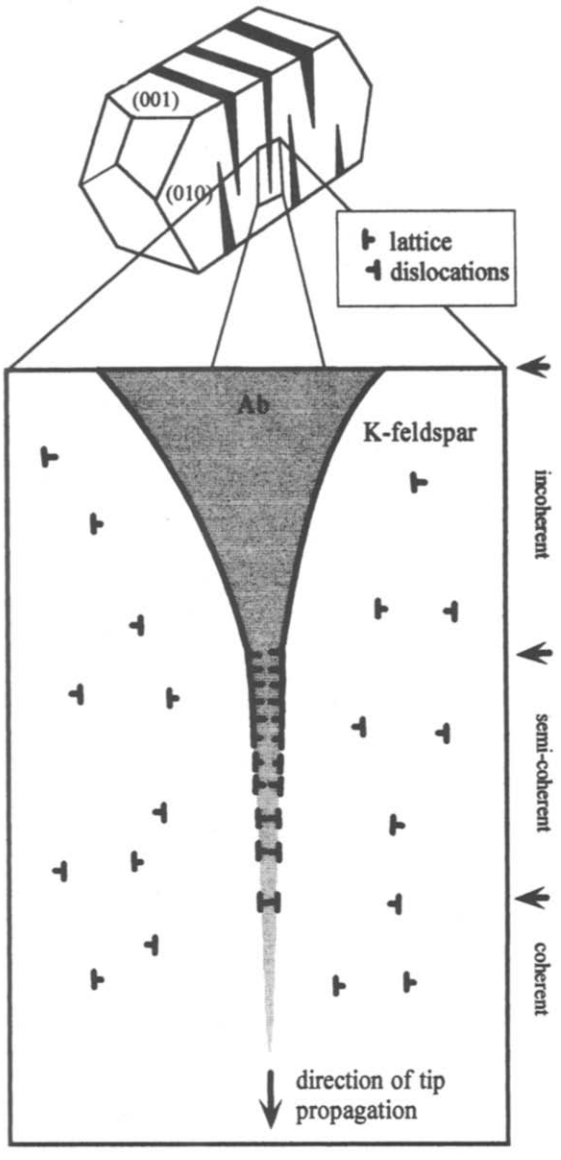


Fig. 6. Model of coherent flame tip propagation that becomes increasingly less coherent away from the tip. The interface may acquire dislocations as it moves through the host.

Albite flames (Fig. 4) preferentially form subparallel to the bulk principal compressive stress direction ($\sigma_1^b$). The high compressive strength of the K-feldspar grains allows the build-up of a high stress, and correspondingly large (in absolute value) elastic strain. Perthitic grains hosting the flames are oriented crystallographically with the Murchison plane sub-parallel to $\sigma_1^b$ (Fig. 5). Topotaxial replacement of K by Na, with minimal lattice disruption within these grains, is thus an efficient way to reduce the strain energy stored elastically in the K-feldspar lattice, since the lattice of the compressed K-feldspar has

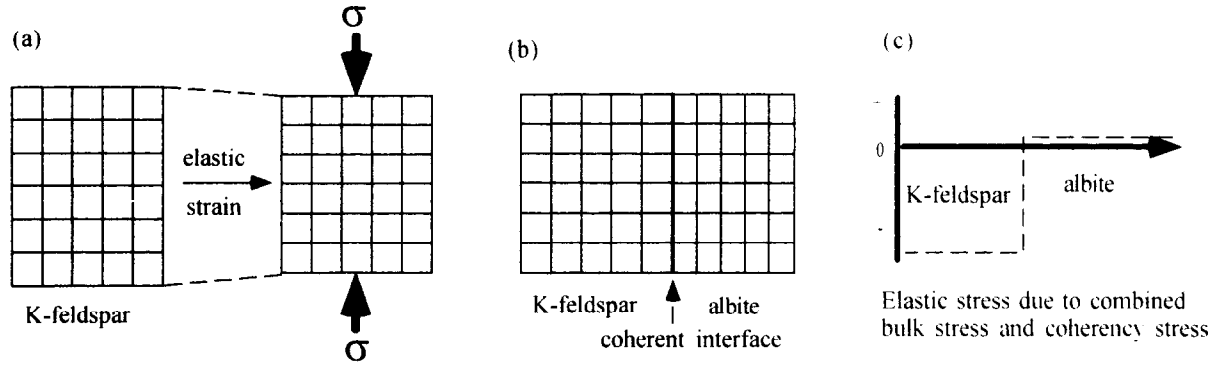


Fig. 7. (a) Schematic representation of strain in a K-feldspar lattice subjected to compressive stress. (b) Coherent interface between stressed K-feldspar and albite. (c) The influence of the external stress on the internal stress distribution, *cf.* Fig. 2(b). Any load applied to the K-feldspar reduces the internal stress in the albite by an equivalent amount such that the stress difference due to coherency remains constant, equivalent to a difference in volume energy of *ca.* 2 kJ mol$^{-1}$.

dimensions close to those of relatively unstrained albite. As long as the flame is oriented parallel to the local maximum compressive stress, the new albite in the K-feldspar is always stressed less than the source plagioclase grain. K moves out of the K-feldspar into a newly grown muscovite that presumably has lower strain energy than the original K-feldspar.

Figure 7(a) shows the elastic stresses in a K-feldspar lattice due to an external tectonic stress. When the external stress is superimposed on the internal coherency stress from Fig. 2 (Fig. 7c) the K-feldspar lattice is highly compressed (−) but the elastic tensional (+) stress in the albite is relatively small. This stress distribution is shown below to energetically favour the development of the flames.

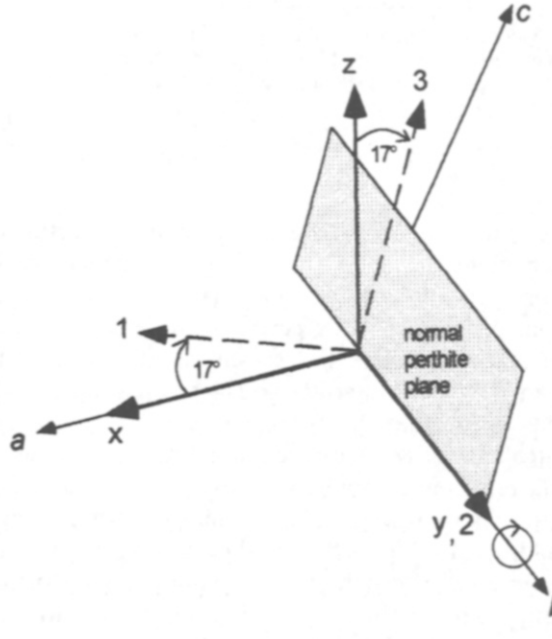


Fig. 8. Coordinate systems. *a, b, c*: conventional crystallographic axes for a monoclinic feldspar (*b* = diad axis). X, Y, Z: conventional cartesian coordinate axes. 1, 2, 3: present choice of cartesian coordinate axes in which the plane of minimum elastic strain energy, i.e. the Murchison plane (shaded), contains the 2 (intermediate) and 3 (minimum) axes. (After Robin 1974.)

*Lattice elastic stresses*

Coherency imposes elastic stresses and strains within the crystal lattice of an isotropically stressed perthite, and these have been calculated in Appendix B and summarised in Table 1. A cartesian co-ordinate system is chosen relative to the Murchison plane (Fig. 8, Robin 1974, Robin 1977). The 1-(maximum strain)-axis is approximately 17° from the *a*-axis and is normal to the Murchison plane. The 2-(intermediate) and 3-(minimum)-axes lie in the Murchison plane; 2 is parallel to the *b*-axis, and 3 is 107° from the *a*-axis, between *a* and *c*, in the crystallographic *ac*-plane.

The difference in elastic stress between the host and coherent lamellae is determined by the difference in lattice parameters between unstressed low albite and microcline or orthoclase (Appendix B). For any given crystallographic direction, this difference is constant regardless of the proportion of albite in the grain (Fig. 9). It is the partitioning of the total lattice elastic stress between the two phases that changes with the amount of albite replacement. In the direction of the 2-axis, the absolute difference in lattice stress, $\Delta_2$ (Fig. 9), is 1.99 GPa for microcline perthites and 2.34 GPa for orthoclase perthites; along the 3-axis this difference, $\Delta_3$, is 0.92 and 0.65 GPa, respectively. The difference in volumetric strain due to coherency between microcline and orthoclase perthites is small; −0.0074 and −0.0075 respectively.

The effect of an external uniaxial stress, $\sigma^b_{1,i}$ (where the subscript *i* indicates along which crystallographic axis, 2 or 3, the stress is directed), is shown in Figs. 9(b) & (c). Compressive (i.e. negative in Fig. 9) stress oriented parallel to the interface will increase the elastic stress in the K-feldspar but decrease stress in the albite by an equivalent amount. As the proportion of albite ($f^{ab}$) increases, so does the fraction of the external stress that must be supported by the remaining K-feldspar. It is apparent from Fig. 9 that, for any external stress between 0 and 1 GPa, there will be some value of $f^{ab}$ for which the directional component of the elastic stress in the coherent albite lamellae is zero. Continued replacement beyond

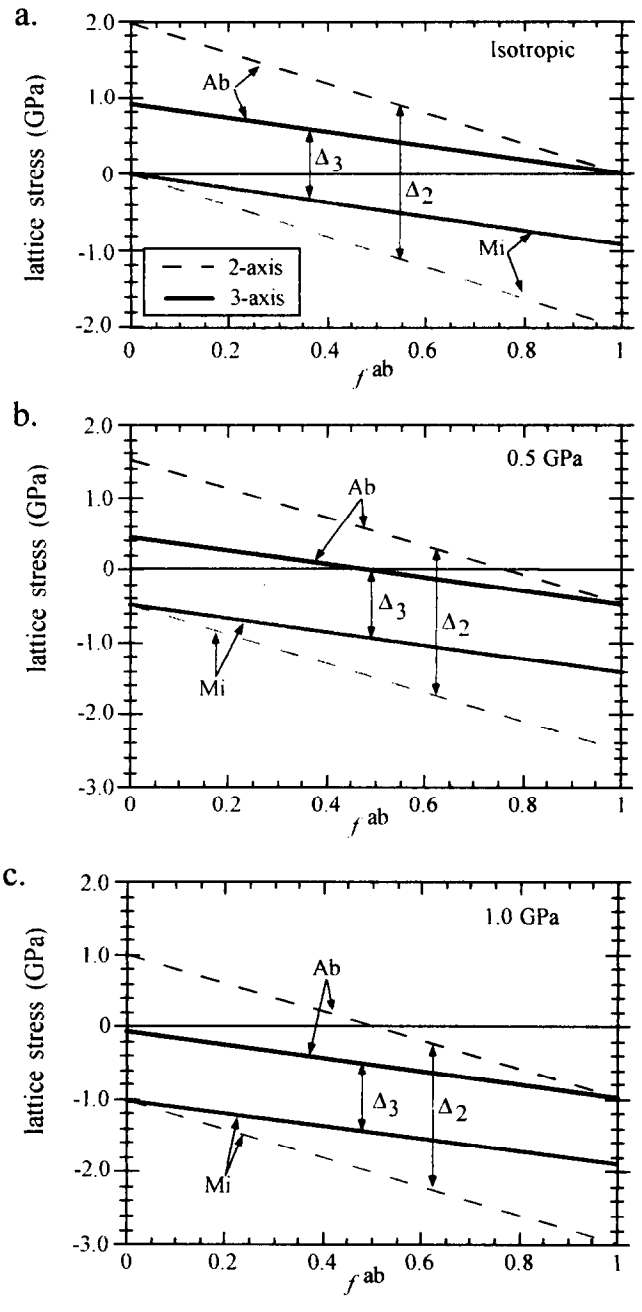


Fig. 9. Lattice stress in albite and microcline relative to the fraction of albite replacement. Solid lines are for stress parallel to the 3-axis and dashed lines, the 2-axis. (a) Isotropic external stress. Compressive (negative) stress due to coherency in microcline starts at 0 and becomes increasingly more negative. Tensional stress in albite reduces to 0 after complete replacement. (b) External stress ($\sigma^b$) of 0.5 GPa. All lines are shifted down relative to the stress-axis or to the left relative to the fraction of replacement compared to (a). Stress in the albite becomes 0 after only 45% (3-axis) or 75% (2-axis) replacement. (c) External stress, $\sigma^b$ = 1.0 GPa. In (a), (b), and (c), $\Delta_2$ = 2.0 GPa; $\Delta_3$ = 0.9 GPa.

this $f^{ab}$ results in compressive stress in the albite, but much smaller than that in the K-feldspar. If replacement continues, however, it is more likely that the flames will partially or completely lose coherency; while the K-feldspar continues to support the external stress, the albite can grow under low or zero net stress.

*Elastic energy (Helmholtz energy)*

The elastic strain energy for albite, microcline ($F^{el,ab}$, $F^{el,mi}$) and the total strain energy, $F_T^{el}$, are calculated in Appendix B and presented in Table 2 and Fig. 10. All of the values plotted in Fig. 10 are with confining pressure, $P_c$ = 0.1 MPa. Column 7 in Table 2 has been calculated for $P_c$ = 0.25 GPa to show that increasing $P_c$ does not significantly change the values in Fig. 10. It is the energy difference between albite and microcline that is important not the absolute energy of either phase.

With $P_c$ alone, the initial elastic energy due to coherency ($F_i^{el}$) is 1.8 kJ mol$^{-1}$ in albite and 0 J mol$^{-1}$ in microcline. The greatest difference in total elastic energy, $\Delta F_T^{el}$, between the maximum, $F_{T_{max}}^{el}$ (at $f^{ab}$ = 0.5), and minimum, $F_{T_{min}}^{el}$ (at $f^{ab}$ = 0 or 1), is 0.45 kJ mol$^{-1}$, and remains the same for all values of $\sigma_{1,i}^b$.

With an external uniaxial compression $\sigma_{1,i}^b$ = 0.5 GPa, $F_i^{el,ab}$ reduces by approximately 0.6 kJ mol$^{-1}$, for stress directed along the 2-axis and 0.3 kJ mol$^{-1}$ for a stress along the 3-axis. This effectively reduces the elastic energy due to coherency in the albite at the initiation of flame growth to 1.2 or 1.5 kJ mol$^{-1}$ respectively. In microcline, $F_i^{el,mi}$ increases to approximately 0.1 and 0.15 kJ mol$^{-1}$ respectively.

When $\sigma_{1,i}^b$ = 1.0 GPa, $F_i^{el,ab}$ is further reduced to 0.75 kJ mol$^{-1}$ for a stress directed along the 2-axis and 1.40 kJ mol$^{-1}$ for stress along the 3-axis. In microcline, $F_i^{el,mi}$ increases to approximately 0.4 and 0.6 kJ mol$^{-1}$ respectively.

In contrast to the reduction in $F_i^{el,ab}$ with compression of the 2- and 3-axes, a compressive stress directed along the 1-axis results in an increase in $F_i^{el,ab}$. For $\sigma_{1,1}^b$ = 0.5 and 1.0 GPa, $F_i^{el,ab}$ increases by 0.76 and 2.26 kJ mol$^{-1}$, respectively.

The elastic energy in microcline increases continuously as replacement proceeds. A critical point, $f_c^{ab}$, is reached when $F^{el,ab} = F^{el,mi}$. Once $f^{ab} > f_c^{ab}$ continued replacement should be energetically favoured since $F^{el,ab} < F^{el,mi}$. With increasing external compressive stress, most notably in the direction of the *b*-axis (2-axis), replacement becomes even more favourable. The value of $f_c^{ab}$ decreases as $\sigma_{1,i}^b$ increases until $f_c^{ab} = 0$ (Fig. 11); for example, when $\sigma_{1,2}^b$ = 1.2 GPa. In this situation, replacement will be highly favoured, since $F^{el,ab} < F^{el,mi}$ for all $f^{ab} > 0$.

The largest source of error in the calculations results from the uncertainty in our knowledge of the elastic constants given in Table B1 (Appendix B). In general, an error of at least 25% can be associated with the uncertainty in the elastic constants. Errors in calculated stress and strain values range from 2% in $\varepsilon_{11}$ to 70% in $\varepsilon_{13}$ (Robin 1974). The effect of pressure and temperature on the results of the stress and strain calculations are discussed in Robin (1974). Generally, the net effect of pressure and temperature should not exceed 20%. Thus, calculated values may be out by as much as 100% and are therefore semiquantitative. The main purpose is to show relative changes in energy between the two feldspars and

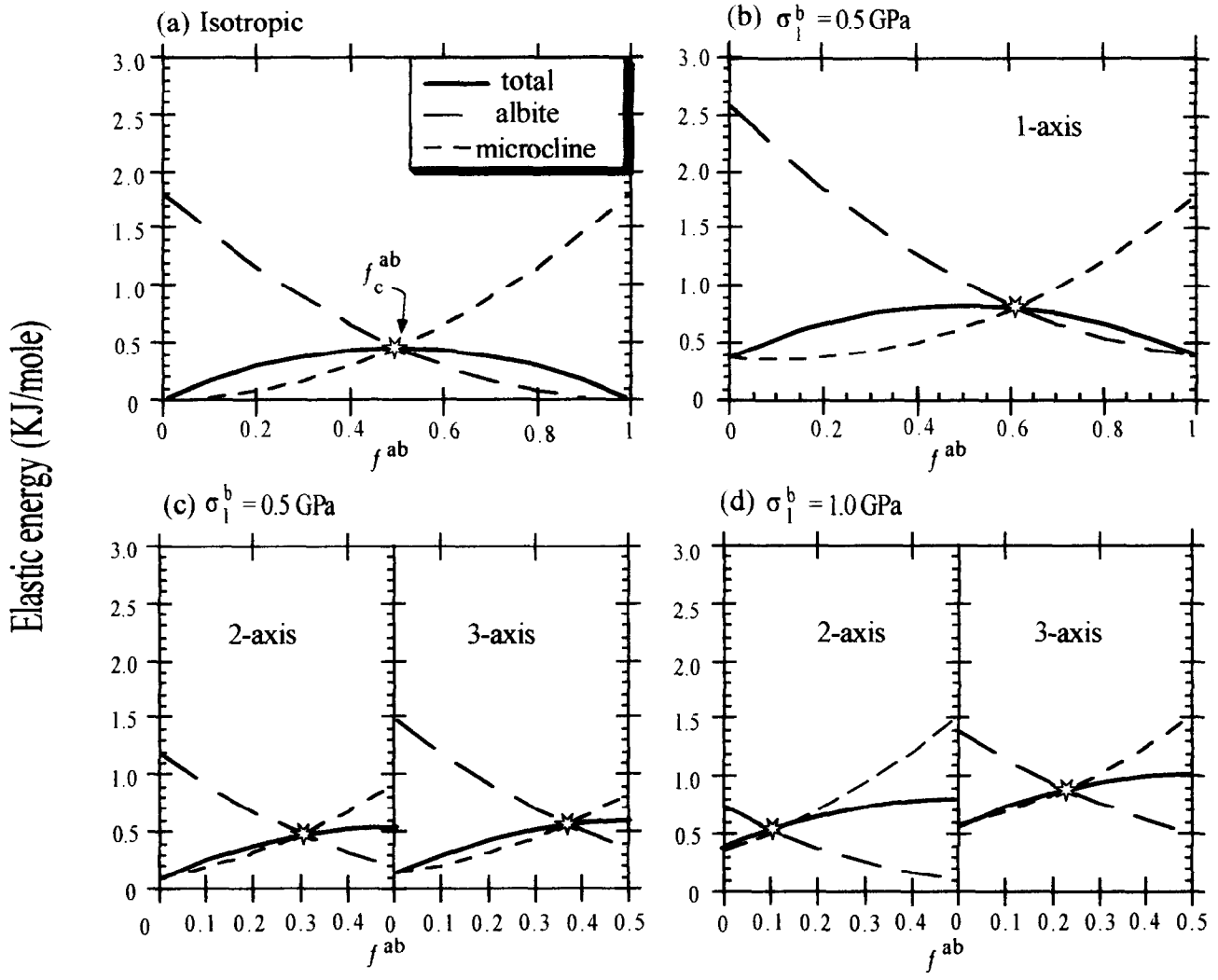


Fig. 10. Total elastic energy (solid line), and the contribution from microcline (short dash) and albite (long dash), of a perthite where $f^{ab}$ is the albite fraction. Total energy is symmetric across $f^{ab} = 0.5$. The point at which the energy in the albite becomes less than that in the K-feldspar, $f_c^{ab}$, is indicated by a star. External differential stress ($\sigma_1^b - \sigma_3^b$) of (a) 0 GPa; (b) 0.5 GPa along the 1-axis; (c) 0.5 GPa along the 2- and 3-axes; (d) 1.0 GPa along the 2- and 3-axes.

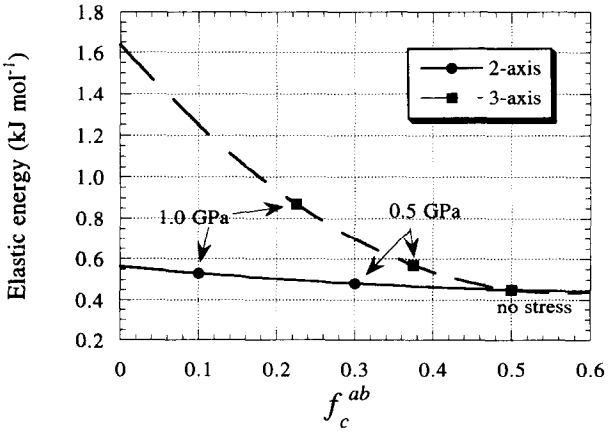


Fig. 11. Plot of the elastic energy at cross-over composition, $f_c^{ab}$, parallel to the 2- (solid line) and 3- (dashed line) axes vs the external differential stress. Increasing $\sigma^b$ parallel to the $b$-axis results in a significant decrease in $f_c^{ab}$, and would be most favourable for flame growth.

in the total and also to illustrate that the model is feasible based on energy constraints.

## DISCUSSION

### *Necessary conditions for stress induced replacement*

This model has been developed following observations made of feldspar replacement in greenschist facies metamorphism in deformed granites. However, it may not require so specific a chemical and/or physical environment to produce albite flames in K-feldspar. The factors that seem most critical for flame growth are as follows.

(1) There must be a stress-related advantage for replacement. High pressure in general would favour albite energetically since the albite unit cell is smaller than that of K-feldspar, with an energy advantage of $P\Delta V$. Stress induced diffusive transfers will occur if the

effect of stress on the chemical potential of K-feldspar is large enough, especially at point contacts between coexisting feldspars where the local stress can be very much higher than the bulk stress. Increasing pressure lowers the energy required for albite replacement.

(2) K-feldspar must act as an unyielding mineral, capable of sustaining high lattice stresses elastically without brittle or plastic deformation. As previously discussed, relatively dry conditions are required in order for the K-feldspar to behave as a rigid object, regardless of temperature. At low metamorphic grade, dry conditions will reduce fracturing while at medium to high grade, dry conditions will inhibit dislocation activity (Tullis & Yund 1980).

(3) There must be an impediment to incoherent boundary formation. Kinetic barriers may result from, for example, sluggish Al–Si diffusion at (i) low temperature and/or (ii) dry conditions (Yund & Tullis 1980).

Therefore, it is possible to envisage this process occurring at temperatures higher than greenschist facies, if there is a source of Na and water pressure is very low. Under such conditions, K-feldspar is strong, Al–Si diffusion is slow and alkali diffusion is relatively rapid (Yund *et al.* 1974).

*Energy requirements for ionic transfers and coherent flame growth*

To understand the amount of energy, in absolute terms, required for a flame perthite grain to form, the $\Delta G$ for 'typical' undercooling of a retrograde reaction can be compared with the strain energy in an elastically stressed microcline. For reaction (1), which has a differential entropy of 0.18 kJ $K^{-1}$ per mole of microcline, an undercooling of 10°C gives a chemical driving force, $\Delta G = 1.8$ kJ $mol^{-1}$. A typical elastic strain energy within a small, strained, coherent albite lamella within an unstrained microcline, is 1.8 kJ $mol^{-1}$, equivalent to undercooling of 10°C. The elastic energy stored in K-feldspar due to external compression of 1.2 GPa is less than 0.6 kJ $mol^{-1}$, depending on stress orientation. Depending on the magnitude of the applied stress, the total strain energy per mole of feldspar in a coherent perthite with $f^{ab} = 0.5$ (Fig. 9) is between 0.45 and 1 kJ $mol^{-1}$. An extra 2–3 kJ $mol^{-1}$ (Brown & Parsons 1993) free energy is involved if the host K-feldspar is orthoclase rather than microcline, which provides more incentive for replacement.

The net energy in the flame perthite depends on (1) the orientation and magnitude of tectonic stress, (2) the extent of replacement, (3) the initial structural state, i.e. ordering, of the K-feldspar, and (4) the degree of coherency, but the energy of complete coherence is typically less than that chemical reactions.

*Coherency stress vs surface energy*

The energy calculations in this model are for coherent lamellae with homogeneous strain. The energies calculated in Appendix B are most realistic for the flame tip, and would therefore be most applicable to the initiation of flame growth, i.e. when $f^{ab} \sim 0$ (Fig. 10, y-intercepts). For an individual flame, the situation is much more complicated once the albite has a finite thickness, with heterogeneous strain in 2 or 3 dimensions in both lattices. Calculations could be done for semi-coherent lamellae with misfit dislocations. There will be a critical lamellar thickness ($t_c$) for which the elastic energy of coherency is equivalent to the energy associated with misfit dislocations on a semi-coherent interface. Near its tip, a flame should widen coherently but lose coherency at width $t_c$ if kinetically possible. Thus, the tip may propagate coherently while the 'wake' progressively loses coherency but inherits the epitaxial relationship with the host.

Lee *et al.* (1995) observe a correlation between lamellar width and etch pit spacing along the interfaces of semi-coherent exsolution lamellae in slowly cooled $Or_{75}$ with $t_c \sim 75$nm. In flame perthites from the GFTZ, we propose that dislocations are introduced at the interface as indicated in Fig. 6, as the interface sweeps through the host, trading a decrease in elastic strain for an increase in surface energy. The value of $t_c$ will increase as the external compressive stress increases as a result of the decrease in lattice spacing in the unreplaced K-feldspar. For very high external stress (> 1 GPa; Fig. 9c), the lattice spacing in K-feldspar may approximate that of albite such that there may be no energy gain associated with a loss of coherency.

## CONCLUSIONS

The combination of retrograde metamorphism of quartzo–feldspathic rocks at greenschist grade and a relatively high differential stress, such as that found in the upper (brittle) level of major crustal shear zones, creates optimal conditions for the development of flame perthite. Some water must be available during the greenschist facies metamorphism but the process of replacement of K-feldspar by perthitic flames of albite is more than one of deuteric alteration. If stress is lower than the brittle strength of K-feldspar, albite flames will form by selective replacement of those K-feldspar grains having a particular crystallographic orientation relative to the strain fabric in the host rock and, by inference, to the tectonic stress field or to the local perturbations of that stress. In general, if a K-feldspar grain is oriented such that the optimum plane for cryptoperthite growth, i.e. plane of minimum lattice misfit between K-feldspar and albite, is parallel to the maximum principal directed stress, then replacement will proceed. If the grain is oriented with the interface plane normal to $\sigma_1$, replacement will be inhibited. Exceptions to this occur where the stress becomes locally reoriented, e.g. contact points between feldspars.

We propose a model for the coherent growth of albite flames by replacement in K-feldspar, in which the K-feldspar lattice planes become elastically compressed as a result of tectonic stress, reducing the proportion of stress due to coherency that the albite lamellae must support. In

growing coherently, the albite saves the energy normally needed to create an incoherent interface or new grain boundary.

*Acknowledgements*—The Natural Sciences and Engineering Research council of Canada made this research possible through an operating grant to P-YR and a scholarship to LLP. We thank Alex C. McLaren, Richard A. Yund and especially John D. Fitz Gerald and an anonymous reviewer for their careful reviews which led to significant improvements to the manuscript.

## REFERENCES

Aberdam, D. 1965. Utilisation de la microscopie électronique pour l'étude des feldspaths. Observations sur des microperthites. *Sci. Terre mem.* **6**, 76.

Bφggild, O. B. 1924. On the labradorization of the feldspars. *Kgl. Danske Vidensk. Selsk. Math. Fys. Medd.* **6**, 1–79.

Bollmann, N. W. & Nissen, H.-U. 1968. A study of optimal phase boundaries: the case of exsolved alkali feldspars. *Acta Cryst.* **A24**, 546–557.

Brown, W. L. & Parsons, I. 1983. Nucleation on perthite–perthite boundaries and exsolution mechanisms in alkali feldspars. *Phys. Chem. Min.* **10**, 55–61.

Brown, W. L. & Parsons, I. 1984. The nature of potassium feldspar, exsolution microtextures and development of dislocations as a function of composition in perthitic alkali feldspars. *Contr. Miner. Petrol.* **86**, 335–341.

Brown, W. L. & Parsons, I. 1993. Storage and release of elastic strain energy: the driving force for low-temperature reactivity and the alteration of alkali feldspar. In *Defects and Processes in the Solid State: Geoscience Applications. The McLaren Volume.* (edited by Boland, J. N. & FiztGerald, J. D.). Elsevier, London. 267–290.

Brown, W. L. & Willaime, C. 1974. An explanation of exsolution orientations and residual strain in cryptoperthites. In *The Feldspars* (edited by Mackenzie, W. S. & Zussman, J.). Manchester University Press. 440–459.

Christie, J. M. & Ord, A. 1980. Flow stress from microstructures of mylonites: examples and current assesment. *J. geophys. Res.* **85**, 6253–6262.

Debat, P., Soula, J. C., Kubin, L. & Vidal, J. L. 1978. Optical studies of natural deformation microstructures in feldspars (gneiss and pegmatites from Occitania Southern France). *Lithos* **11**, 133–145.

Fitz Gerald, J. D. & Stünitz, H. 1993. Deformation of granitoids at low metamorphic grade I: reactions and grain size reduction. *Tectonophysics* **221**, 269–297.

Gandais, M., Guillemin, C. & Willaime, C. 1974. Study of boundaries in cryptoperthites. In *Electron Microscopy. Eighth international congress on electron microscopy.* The Australian Acadamy of Science, Canberra, 508–509.

Haggart, M. J., Jamieson, P. H., Reynolds, P. H., Krogh, T. E., Beaumont, C. & Culshaw, N. G. 1993. Last gasp of the Grenville Orogeny: thermochronology of the Grenville Front Tectonic Zone near Killarney, Ontario. *J. Geol.* **101**, 575–589.

Handy, M. R. 1994. Flow laws for rocks containing two non-linear viscous phases: a phenomenological approach. *J. Struct. Geol.* **16**, 287–301.

Laves, F. 1952. Phase relations of the alkali feldspars II. *J. Geol.* **60**, 549–574.

Lee, M. R., Waldron, K. A. & Parsons, I. 1995. Exsolution and alteration microtextures in alkali feldspar phenocrysts from the Shap granite. *Miner. Mag.* **59**, 63–78.

Martin, R. J. 1972. Time-dependent crack growth in quartz and its application to the creep of rocks. *J. geophys. Res.* **77**, 1406–1419.

Nye, J. F. 1957. *Physical Properties of Crystals.* Oxford University Press, London.

O'Donnell, L. L. 1986. Characterization of the nature of deformation and metamorphic gradient across the Grenville Front Tectonic Zone in Carlyle Township, Ontario. Unpublished M.Sc. Thesis, McMaster University, Hamilton, Ontario.

Orville, P. M. 1967. Unit cell parameters of the microcline–low albite and the sanidine–high albite solid solution series. *Am. Miner.* **52**, 55–86.

Passchier, C. W. 1982. Mylonitic deformation in the Saint-Barthélemy Massif, French Pyrenees. G. U. A. Paper of Geol. 1, No. 16, 173pp.

Petrović, R. 1973. The effect of coherency stress on the mechanism of the reaction albite $+K^+$ K-feldspar $+Na^+$ and on the mechanical state of the resulting feldspar. *Contr. Miner. Petrol.* **41**, 151–170.

Pryer, L. L. 1985. Preliminary report on the Grenville Front Tectonic Zone, Carlyle Township, Ontario. In *Studies in the Grenville Province of Ontario. Current Research, Part A, Geol. Survey Canada,* (edited by Davidson, A., Nadeau, L., Grant, S. M., & Pryer, L. L.) Paper 85-1A, 463–483.

Pryer, L. L. 1993. Microstructures in feldspars from a major crustal thrust zone: the Grenville Front, Ontario, Canada. *J. Struct. Geol.* **15**, 21–36.

Pryer, L. L. & Robin, P.-Y. F. 1995. Retrograde metamorphic reactions in deforming granites and the origin of flame perthite. *J. Met. Geol.* **14**, 645–658.

Pryer, L. L., Robin, P.-Y. F. & Lloyd, G. E. 1995. SEM electron channelling study of flame perthite. *Can. Miner.* **33**, 333–347.

Ranalli, G. & Murphy, D. C. 1987. Rheological stratification of the lithosphere. *Tectonophysics* **132**, 281–295.

Robin, P.-Y. F. 1974. Stress and strain in cryptoperthite lamellae and the coherent solvus of alkali feldspars. *Am. Miner.* **59**, 1299–1318.

Robin, P.-Y. F. 1977. Angular relationships between host and exsolution lamellae and the use of the Mohr circle. *Am. Miner.* **62**, 127–131.

Ryzhova, T. V. & Aleksandrov, K. S. 1965. The elastic properties of potassium–sodium feldspars. In *Bull. (Izv.) Acad. Sci. USSR, Geophys. Ser.*, 98-102. *Am. Geophys. Union Trans.*, 53–56.

Ryzhova, T. V. 1964. The elastic properties of plagioclase. *Bull. (Izv.) Acad. Sci. USSR, Geophys. Ser.*, 1049-1051. *Am. Geophys. Union Trans.*, 633–635.

Sacerdoti, M., Labernardière, H. & Gandais, M. 1980. Transmission electron microscope (TEM) study of geologically deformed potassic feldspars. *Bull. Miner.* **103**, 148–155.

Simpson, C. 1985. Deformation of granitic rocks across the brittle–ductile transition. *J. Struct. Geol.* **7**, 503–511.

Smith, J. V. 1961. Explanation of strain and orientation effects in perthites. *Am. Miner.* **46**, 1489–1493.

Smith, J. V. 1974. *Feldspar Minerals 2. Chemical and Textural Properties.* Springer-Verlag, Berlin.

Smithson, S. B. 1963. Granite studies II. The Precambrian Flå granite, a geological and geophysical investigation. *Norges Geologiske Undersøkelsce* **219**, 212.

Stel, H. 1986. The effect of cyclic operation of brittle and ductile deformation on the metamorphic assemblages in cataclasites and mylonites. *PAGEOPH* **124**, 289–307.

Tullis, J. & Yund, R. A. 1980. Hydrolytic weakening of experimentally deformed Westerly granite and Hale albite rock. *J. Struct. Geol.* **2**, 439–451.

Tullis, J. & Yund, R. A. 1977. Experimental deformation of dry Westerly granite. *J. geophys. Res.* **82**, 5705–5718.

Tullis, J. & Yund, R. A. 1992. The brittle–ductile transition in feldspar aggregates: an experimental study. In *Fault Mechanics and Transport Properties of Rocks*, (edited by Evans, B. & Wong, T.-F.). Academic Press, San Diego, CA. 89–117.

Tullis, J., Shelton, G. L. & Yund, R. A. 1979. Pressure dependence of rock strength: Implications for hydrolytic weakening. *Bull. Miner.* **102**, 110–114.

Twiss, R. J. 1977. Theory and applicability of a recrystallized grain size palaeopiezometer. *Pure appl. Geophys.* **115**, 227–244.

Vernon, R. H., Williams, V. A. & D'Arcy, W. F. 1983. Grain-size reduction and foliation development in a deformed granitoid batholith. *Tectonophysics* **92**, 123–145.

Willaime, C., Brown, W. L. & Gandais, M. 1973. An electron microscopic and X-ray study of complex exsolution textures in a cryptoperthitic alkali feldspar. *J. Mater. Sci.* **8**, 461–466.

Willaime, C., Christie, J. M. & Kovacs, M.-P. 1979. Experimental deformation of K-feldspar single crystals. *Bull. Miner.* **102**, 168–177.

Windley, B. F. 1986. Comparative tectonics of the western Grenville and western Himalaya. In *The Grenville Province*, (edited by Moore, J. M., Davidson, A. & Baer, A. J.). GAC Special Paper 31, 341–348.

Wright, T. L. & Stewart, D. B. 1968. X-ray and optical study of alkali feldspar. I. Determination of composition and structural state from refined unit cell parameters and 2V. *Am. Miner.* **53**, 38–87.

Wynne-Edwards, H. R. 1972. The Grenville Province. In *Variations in Tectonic Styles in Canada*, (edited by Price, R. A. & Douglas, R. J. W.). Geological Association of Canada Spec. Paper 11, 263–334.

Yund, R. A. 1983. Microstructure, kinetics and mechanisms of alkali feldspar exsolution. In *Feldspar Mineralogy, 2nd Edition*, (edited by Ribbe, P. H.) *Miner. Soc. Am., Rev. Min.* **2**, 177–202.

Yund, R. A. & Tullis, J. 1980. The effect of water, pressure, and strain on Al/Si order– disorder kinetics in feldspar. *Contr. Miner. Petrol.* **72**, 297–302.

Yund, R. A., McLaren, A. C. & Hobbs, B. E. 1974. Coarsening kinetics of the exsolution microstructure in alkali feldspar. *Contr. Miner. Petrol.* **48**, 45–55.

## APPENDIX A

*Palaeopiezometry using quartz*

The use of dynamically recrystallised quartz-grain-size as an indication of the magnitude of the imposed differential stress at the time of recrystallisation has been reviewed by Twiss (1977) and Christie & Ord (1980). The success of this method relies heavily on the preservation of the dynamically recrystallised grain-size through relatively rapid and static cooling. Thrust faulting is likely to produce such conditions.

The differential stress has been estimated in samples used in this study, through this palaeopiezometer (Table A). Grain size was estimated using a petrographic microscope; the average minimum grain size measured within a quartz ribbon or on the boundary of a dynamically recrystallised quartz grain was taken to be the size indicative of the differential stress at the time of deformation (Twiss 1977). Differential stresses range from 0.2–0.3 GPa, corresponding to the flow stress for quartz under greenschist facies conditions.

Table A. Quartz grain size paleopiezometry

| Sample* | Grain Size ($\mu$m) | $\sigma_1-\sigma_3$ (MPa) |
|---|---|---|
| P231 | 5 | 280 |
| P115 | 7 | 267 |
| P368 | 10 | 250 |
| P460 | 8 | 261 |
| P139 | 10 | 250 |
| P268 | 10 | 250 |
| P102 | 20 | 218 |

*Sample locations are listed here in order of increasing metamorphic grade $(\sigma_1-\sigma_3) = AD^{-n}$, D = recrystallized grain size, A = 603MPa, n = 0.68, (Twiss 1977).

## APPENDIX B

*Stresses and strains within coherent flame perthites*

The stress and strain values calculated below for low albite–microcline perthites are presented in Table 1. The values calculated by Robin (1974) for high albite–sanidine are given for comparison.

*Stress-free compositional strains*

The lattice strain imposed due to coherency between a pure K-feldspar host and an albite lamellae can be simply determined using the difference in unit cell parameters for the end member compositions. The lattice parameters for microcline (Orville 1967) and orthoclase (Wright & Stewart 1968) are:

$a^{mi} = 8.589$, $a^{or} = 8.606$, $b^{mi} = 12.963$, $b^{or} = 13.000$, $c^{mi} = 7.223$, $c^{or} = 7.200$, $b^{mi} = 115.95°$; $b^{or} = 115.92°$

and for albite (Orville 1967):

$a^{ab} = 8.142$, $b^{ab} = 12.781$, $c^{ab} = 7.155$, $b^{ab} = 116.67°$.

Taking the host K-feldspar lattice as the reference state, the lattice strain can be defined by: $\Delta a/a^{mi} = (a^{mi}-a^{ab})/a^{mi} = 0.0520$, $\Delta a/a^{or} = 0.0539$.

Similarly, $\Delta b/b^{mi} = 0.0140$; $\Delta c/c^{mi} = 0.0094$; $\Delta b^{mi} = 0.72° = 0.0125$ rad.

$\Delta b/b^{or} = 0.0168$; $\Delta c/c^{or} = 0.0062$; $\Delta b^{or} = 0.72° = 0.0130$ rad.

The compositional strain coefficients (Robin 1974) for coherent perthite lamellae are determined using the values above. The *b*-axis is the intermediate principal axis of strain. The minimum principal axis of strain is in the *ac*-plane and can be determined by Mohr circle (Robin 1977). The strain coefficients in this coordinate system ($\eta_{ij}$) for low albite–microcline perthites and, for comparison, low albite–orthoclase perthites (all values given in brackets for the remainder of the calculations) have the values:

$\eta_{11} = 0.0585$ (0.0607); $\eta_{22} = 0.0140$ (0.0168); $\eta_{33} = 0.0091$ (0.0057); $\eta_{11}+\eta_{22}+\eta_{33} = 0.0816$ (0.0832).

Elasticity calculations for coherent albite lamellae formed by replacement within low-temperature K-feldspars differ from those for high albite–sanidine cryptoperthite (Robin 1974) in three respects:

(1) The compositional strains must be calculated from different lattice parameters;

(2) The coexisting phases are near pure albite and microcline, and, in first approximation, stay fixed during replacement;

(3) The average composition of the feldspar grains, $X°$, changes during replacement.

*Stresses and strains*

In a coherent perthite, the host and lamellae are elastically constrained to match the lattice of the average crystal. The elastic strain components imposed by coherency are:

$$\varepsilon_3 = \varepsilon_{33} = -\eta_{33} = -0.0091(-0.0057), \quad (3a)$$

$$\varepsilon_2 = \varepsilon_{22} = -\eta_{22} = -0.0140(-0.0168), \quad (3b)$$

$$\varepsilon_4 = 2\varepsilon_{23} \approx 0. \quad (3c)$$

This strain is distributed between the host and lamellae in proportion to the fraction of host crystal that has been replaced.

Stress and strain are related by Hooke's Law (Nye 1957), i.e.:

$\sigma_i = c_{ij}\varepsilon_j$; $c_{ij}$ = stiffness, $\sigma_i$ = lattice stress.

Stiffness coefficients for alkali feldspars determined by Ryzhova & Aleksandrov (1965), recalculated into the coordinate system (Fig. 8) by Robin (1974, Table B1) have been used to calculate the remaining strain and stress values. The solution to Hooke's equations gives the following elastic stresses and strains:

$$\sigma_1 = \sigma_4 = \sigma_5 = \sigma_6 = 0;\ \varepsilon_4 = \varepsilon_6 = 0, \quad (4a)$$

$$\sigma_{33} = \sigma_3 = -0.92(-0.65)\,\text{GPa}, \quad (4b)$$

$$\sigma_{22} = \sigma_2 = -1.99(-2.34)\,\text{GPa}, \quad (4c)$$

$$\varepsilon_{11} = \varepsilon_1 = +0.0157(+0.0150), \quad (4d)$$

$$2\varepsilon_{13} = \varepsilon_5 = -0.0021(-0.0028), \quad (4e)$$

and the volumetric strain is:

$$\varepsilon_1+\varepsilon_2+\varepsilon_3 = -0.0074(-0.0075).$$

For the low albite–microcline perthite, the directional components for lattice stress under hydrostatic conditions are (Fig. 7a):

$$\sigma_2^{ab} - \sigma_2^{mi} = 1.99(2.34)\,\text{GPa}, \quad (5a)$$

$$\sigma_3^{ab} - \sigma_3^{mi} = 0.92(0.65)\,\text{GPa}. \quad (5b)$$

The proportion of this stress sustained by the albite and the K-feldspar lattices, depends on the fraction, *f*, of each of the two phases. With the additional application of an external uniaxial stress, the stresses for both albite and microcline can be resolved into directional components along the 2- and 3-directions and must equal the externally applied stress.

$$f^{ab}\sigma_2^{ab} + f^{mi}\sigma_2^{mi} = \sigma_{1.2}^b, \quad (6a)$$

$$f^{ab}\sigma_3^{ab} + f^{mi}\sigma_3^{mi} = \sigma_{1.3}^b, \quad (6b)$$

where $\sigma_i^{ab}$, $\sigma_i^{mi}$ are the lattice stresses of albite and microcline lamellae respectively and $\sigma_{1.i}^b$ is the external stress parallel to direction *i* within the crystal.

Combining equations (5) and (6) and substituting $(1-f^{ab})$ for $f^{mi}$, the directional components in terms of the amount of replacement become:

$$\sigma_2^{ab} = \sigma_{1.2}^b -, 1990(f^{ab}-1),$$

$$\sigma_3^{ab} = \sigma_{1.3}^b - 920(f^{ab}-1),$$

$$\sigma_2^{or} = \sigma_{1.2}^b - 1990(f^{ab}),$$

$$\sigma_3^{or} = \sigma_{1.3}^b - 920(f^{ab}).$$

Table B1. Selected stiffness coefficients of alkali feldspars

| $c_{ij}$ | 11 | 12 | 13 | 22 | 23 | 33 | 15 | 44 | 25 | 55 | 35 | 66 | 46 |
|---|---|---|---|---|---|---|---|---|---|---|---|---|---|
| No. 61* | 0.596 | 0.362 | 0.360 | 1.581 | 0.285 | 1.049 | −0.118 | 0.139 | −0.057 | 0.203 | −0.129 | 0.370 | −0.026 |
| C† | 0.750 | 0.430 | 0.490 | 1.720 | 0.360 | 1.280 | −0.170 | −0.170 | −0.140 | 0.300 | −0.190 | 0.370 | −0.030 |
| No. 61‡ | 0.493 | 0.324 | 0.364 | 1.581 | 0.326 | 1.145 | −0.050 | 0.173 | −0.069 | 0.207 | −0.028 | 0.336 | −0.086 |
| C‡ | 0.615 | 0.346 | 0.469 | 1.720 | 0.444 | 1.457 | −0.054 | 0.204 | −0.136 | 0.279 | −0.096 | 0.336 | −0.081 |

*Ryzhova & Aleksandrov (1965), Table 3. Conventional coordinates. †Composite set of elastic coefficients from Ryzhova & Aleksandrov (1965), Table 3, and from Ryzhova (1964). Conventional coordinates. ‡Elastic coefficients recalculated in new coordinate system, illustrated in Fig. 8, from Robin (1974).

*Elastic strain energy*

The elastic strain energy per unit volume ($F^{el}$) is defined as:

$$F^{el} = \frac{1}{2}\sigma_j\varepsilon_i,$$

where the superscript, *el*, refers to elastic energy. The choice of axes, i.e. with 2 principal axes within the plane of the lamellae and one normal to it, means that there are only 2 non-zero stresses, which simplifies the expression of the total elastic energy per unit volume ($F_T^{el}$) equation to:

$$F_T^{el} = \frac{1}{2}(\sigma_2\varepsilon_2 + \sigma_3\varepsilon_3).$$

Using the values calculated above gives the elastic strain energy for the end-member albite–microcline pair in an isotropically stressed cryptoperthite of:

$$F_T^{el} = 18.1 \text{ MPa}.$$

The total Helmholtz energy equation per unit volume ($F_T^{el,b}$) in the presence of an external stress can be written in terms of the extent of Ab replacement as:

$$F_T^{el,b} = f^{ab}F^{el,ab} + f^{or}F^{el,\,or}.$$

This expands to:

$$F_T^{el,b} = \frac{1}{2}[(f^{ab})(\sigma_2^{ab}\varepsilon_2 + \sigma_3^{ab}\varepsilon_3) + (1 - f^{ab})(\sigma_2^{mi}\varepsilon_2 + \sigma_3^{mi}\varepsilon_3)].$$

Strain for various stresses along the 2- and 3-directions ($\varepsilon_i^b$) (Table B2), calculated using Hooke's equation and the compressibility coefficients (Table B1), are added to the compositional strains from equation (3) to give the total strain:

$$\varepsilon_2^{ab} = -0.0140(f^{ab} - 1) + \varepsilon_2^b,$$

$$\varepsilon_3^{ab} = -0.0091(f^{ab} - 1) + \varepsilon_3^b,$$

$$\varepsilon_2^{mi} = -0.0140(f^{ab}) + \varepsilon_2^b,$$

$$\varepsilon_3^{mi} = -0.0091(f^{ab}) + \varepsilon_3^b.$$

Table B2. Lattice elastic strain due to external stress $\sigma_{1,i}{}^b$

| Stress direction | 1-axis | | 2-axis | | 3-axis | |
|---|---|---|---|---|---|---|
| $\sigma_{1,i}{}^b$ (GPa) | 0.5 | 1.0 | 0.5 | 1.0 | 0.5 | 1.0 |
| $\varepsilon_2{}^b$ ($\times 10^4$) | +20.9 | +41.7 | −37.0 | −73.9 | +3.7 | +7.5 |
| $\varepsilon_3{}^b$ ($\times 10^4$) | +40.3 | +80.6 | +3.7 | +7.5 | −57.5 | −114.9 |

Note that all stresses are compressional.
Extensional strain (+), compressional strain (−).